

Effects of the low-frequency zonal wind variation on the high frequency atmospheric variability over the tropics

K. P. Sooraj · Daehyun Kim · Jong-Seong Kug · Sang-Wook Yeh · Fei-Fei Jin · In-Sik Kang

Received: 13 March 2008 / Accepted: 9 October 2008 / Published online: 26 October 2008
© Springer-Verlag 2008

Abstract Recently, there is increasing evidence on the interaction of atmospheric high-frequency (HF) variability with climatic low-frequency (LF) variability. In this study, we examine this relationship of HF variability with large scale circulation using idealized experiments with an aqua-planet Atmospheric GCM (with zonally uniform SST), run in different zonal momentum forcing scenarios. The effect of large scale circulation changes to the HF variability is demonstrated here. The HF atmospheric variability is enhanced over the westerly forced region, through easterly vertical shear. Our study also manifests that apart from the vertical wind shear, strong low-level convergence and horizontal zonal wind shear are also important for enhancing the HF variance. This is clearly seen in the eastern part of the forcing, where the HF activity shows relatively maximum increase, in spite of similar vertical shear over the forced regions. The possible implications for multi-scale interaction (e.g. MJO–ENSO interaction) are also discussed.

Keywords ENSO/MJO interaction · Scale interaction · High-frequency variability · Aqua-planet experiments · State-dependent noise

1 Introduction

The westerly wind events (WWEs) have been observed to occur in association with the onset of most El Niño event for the past 50 years (Kerr 1999; McPhaden 1999, 2004). The importance of this interaction between, ENSO and relatively shorter-timescale atmospheric variability such as the Madden and Julian Oscillation (MJO) and WWEs, is recently supported by several theoretical and modeling studies (Lengaigne et al. 2004; Eisenman et al. 2005; Perez et al. 2005; Zavala-Garay et al. 2005; Jin et al. 2007; Gebbie et al. 2007). These studies indicate a two-way interaction between ENSO-related SST anomaly and HF atmospheric variability, while other studies (e.g. Kessler and Kleeman 2000; Gebbie et al. 2007) imply a dependency of high frequency (HF) atmospheric variability or atmospheric noise (e.g. WWEs) upon slowly varying large-scale anomalous features such as SST. Moreover, many studies have suggested that not only ENSO is dependent on fast HF atmospheric variability, but MJO and WWE activity gets itself modulated by temperature anomalies in the central equatorial Pacific (Keen 1982; Luther et al. 1983; Gutzler 1991; Kessler and Kleeman 2000; Vecchi and Harrison 2000; Yu et al. 2003; Eisenman et al. 2005; Perez et al. 2005). In particular, recently, Kug et al. (2008a, b), showed a clear statistical relationship between NINO3.4 SST and activity of HF atmospheric variability. They demonstrated that the strong activity of HF atmospheric variability such as synoptic eddy, WWEs, and MJO is simultaneously found during the ENSO warm phase over

K. P. Sooraj · D. Kim · I.-S. Kang
Climate Environment System Research Center,
Seoul National University, Seoul, South Korea

J.-S. Kug (✉) · F.-F. Jin
School of Ocean and Earth Sciences and Technology,
University of Hawaii, Manoa, 2525 Correa Road,
HIG 350, Honolulu, HI 96822, USA
e-mail: kug@hawaii.edu; jskug@climate.snu.ac.kr

S.-W. Yeh
Korea Ocean Research and Development Institute,
Ansan, South Korea

the central Pacific. Therefore, their statistical results support the notion that HF atmospheric variability depends on the state of ENSO. However, so far it is not clear how the HF atmospheric variability is controlled by the ENSO.

Recent studies, interestingly, suggest an interaction of HF atmospheric variability with the atmospheric low-frequency (LF) oscillation. Maloney and Hartmann (2001) have shown that the westerly phase of MJO favors the growth of small scale, slow moving synoptic eddy disturbances. Also, Seiki and Takayabu (2007a, b) showed recently that WWEs tends to occur frequently under LF environmental westerlies. They suggested a mechanism for synoptic-scale eddy development in the generation of WWEs over the western and central Pacific under LF environmental westerlies, by analyzing eddy kinetic energy (EKE) budget. They further argued that the WWEs frequently occur in the westerly phase of MJO as well as in El Nino phase.

Kug et al. (2008a, b) recently showed a clear statistical relationship between LF zonal wind variation and activity of HF atmospheric variation, both in observational and model-simulated data. It is well known that the ENSO system largely controls LF wind variability over the tropical Pacific. Therefore, according to them, during El Nino onset and peak phases, the anomalous westerlies associated with El Nino, intensify the WWE/MJO interaction over the western-central Pacific. Also, these LF westerlies give a favorable condition for strong HF atmospheric variability, thus indicating both WWE and MJO activity is amplified under the El Nino related background westerlies. So, they suggested that the HF atmospheric variability associated with ENSO (so called state-dependent atmospheric noise) is rather dependent on the atmospheric LF wind field than SST.

The arguments and conclusions of above studies were based mainly on statistical analysis and so are subjected to the limitation of statistical analysis. It is still unclear how the HF atmospheric variability is dynamically controlled by its LF counterpart and experimental modeling may help us to understand it better. To date, however, any systematic modeling experiments have not been undertaken to study it. However, in order to assess the importance of specific dynamical interactions or feedbacks, it is essential to use the models with simplified settings and in which some interactions are either greatly simplified or ignored. Aqua-planet simulations are one basic tool to study this.

The objective of this study is to investigate the interaction between LF zonal wind and HF atmospheric variability in a global climate model. Here, we will use the SNU AGCM for examining this interaction. Our approach relies mainly on the idealized experiments with an aqua-planet AGCM (with zonally uniform SST) run in different westerly momentum forcing scenarios.

The organization of this paper is as follows. In Sect. 2, the data, the model used and model experiment details are described. Section 3 analyses the relationship of HF atmospheric variability with large scale circulation in observation and models. Section 4 gives the results based on the aqua planet experiments. The summary and discussion is given in Sect. 5.

2 Models, data and experiments

2.1 Model descriptions

The models used in this study are the Seoul National University atmospheric GCM (SNU AGCM) and coupled GCM (SNU CGCM, Kug et al. 2008c). The SNU AGCM is a global spectral model, with 20 vertical levels in a sigma coordinate. Horizontal resolution T42 version is used. The deep convection scheme is a simplified version of the relaxed Arakawa–Schubert (SAS) scheme (Numaguti et al. 1995). The large-scale condensation scheme consists of a prognostic microphysics parameterization for total cloud liquid water (Le Treut and Li 1991) with a diagnostic cloud fraction parameterization. A non-precipitating shallow convection scheme (Tiedtke 1983) is also implemented in the model for mid-tropospheric moist convection. The boundary layer scheme is a non-local diffusion scheme based on Holtslag and Boville (1993), while the land surface model is from Bonan (1996). The radiation process is parameterized by the two-stream k distribution scheme implemented by Nakajima et al. (1995).

Observational (Stevens 1979) and numerical studies (Stevens et al. 1977; Stones et al. 1974) indicate that the CMT is an important mechanism of momentum exchange in tropical disturbances and also for realistic simulation of tropical circulation. Hence, in this study, the CMT parameterization as suggested by Wu and Yanai (1994), is implemented. The present parameterization of the CMT was developed based on Eqs. 19 and 20 in Wu and Yanai (1994). Detailed descriptions of the implemented parameterization can be found in Kim et al. (2008).

The CGCM used here was developed at SNU with the same atmospheric component as the AGCM. The oceanic component is the MOM2.2 Oceanic GCM developed at the Geophysical Fluid Dynamics Laboratory (GFDL). The model is a finite difference treatment of the primitive equations of motion using the Boussinesq and hydrostatic approximations in spherical coordinates. The domain of the model covers most global oceans, and its coastline and bottom topography are realistic. The zonal resolution is 1.0° . The meridional grid spacing between 8°S and 8°N is $1/3^\circ$, gradually increasing to 3.0° at 30°S and 30°N , and is fixed at 3.0° in the extratropics. There are 32 vertical

levels with 23 levels in the upper 450 m. In the CGCM, a mixed layer model, developed by Noh and Kim (1999) is embedded in the ocean model to improve the climatological vertical structure of the upper ocean.

The ocean model communicates once a day with the atmospheric model. The two component models exchange the following data: SST, wind stress, freshwater flux, longwave and shortwave radiation, and turbulent fluxes of sensible and latent heat. Although no flux correction is applied, the model does not exhibit a significant climate drift in the long-term simulation. In addition, the CGCM reasonably simulates the climatology of most oceanic and atmospheric variables (Kug et al. 2008c; Kim et al. 2008). Moreover, Kug et al. (2008b) has compared the model simulation of ENSO with HF variability.

The AGCM is integrated from 1979 to 1999 with observed SST as a boundary condition. The CGCM is integrated over 50 years.

2.2 Data

The observational data used in this study are SST (monthly means) and zonal winds (daily and monthly means) for the period of 1979–1999, the same as that of the AGCM simulation period. The monthly mean SST data are from the improved extended reconstructed sea surface temperature version 2 (ERSST.v2) data set (Smith and Reynolds 2004) created by the National Climate Data Center (NCDC).

The daily and monthly wind data are taken from the National Center for Environmental Prediction/National Center for Atmospheric Research (NCEP/NCAR, Kalnay et al. 1996). Daily anomalies are obtained after removing the climatological annual cycle, which is obtained by averaging all the daily data on the same calendar dates. A 2–90 day band-pass LANCZOS filter (using 45 weights, Duchon 1979) is applied to the daily zonal wind anomalies at 925 hPa level, in order to investigate HF atmospheric variability. We extended the same analysis to the model generated zonal winds and SST. But in the model, we used only wind at 850 hPa, being the lowest available level of atmospheric circulation in the model. Hereafter, the variability of the filtered wind (both in the model and observation) is referred to as HF variability for simplicity. The variance of the filtered wind, SST and zonal wind are smoothed using a 3 month moving window. Further, they are interpolated to a coarse resolution of $5 \times 5^\circ$ to focus on the large scale circulation features.

2.3 Experimental design

As discussed in the introduction it is still unclear how the atmospheric HF variability is dynamically controlled by LF

wind, though there were some studies based on the statistical analyses (Kug et al. 2008b). So far, there are few studies for understanding the dynamics behind this interaction. So, we here conducted a set of idealized aqua-planet experiments (Neale and Hoskins 2000), since it is more useful to interpret the responses of the model to different momentum forcing. Further, it will enable us to better understand the interaction between tropical eddy disturbances and large scale atmospheric variability.

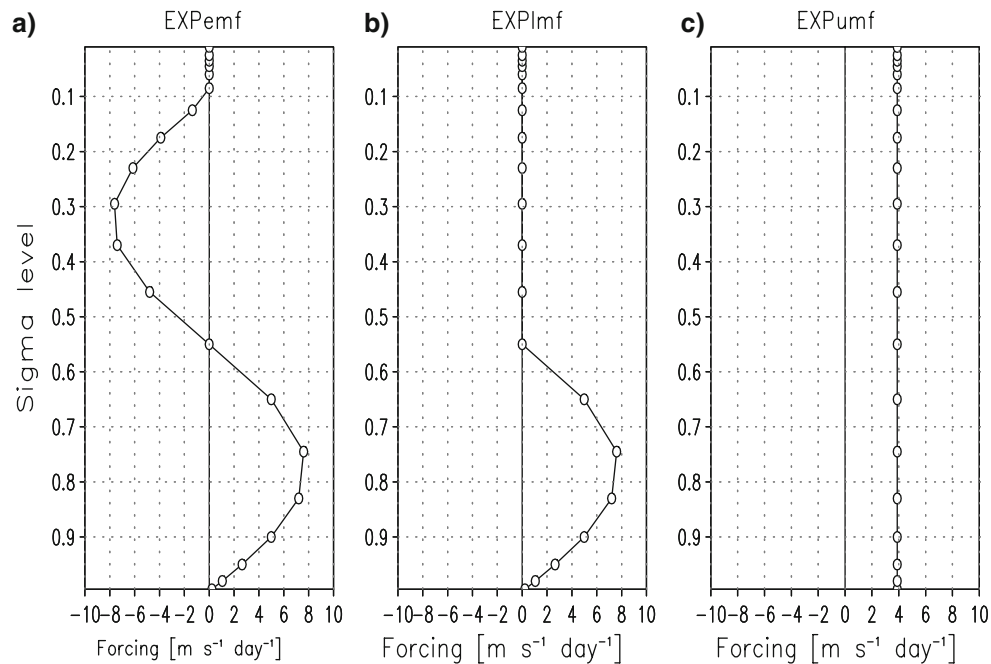
We performed aqua-planet experiments with the SNU AGCM. Most of the experimental design follows the detailed specifications proposed by Neale and Hoskins (2000). For the distribution of insolation at the top of the atmosphere, perpetual solar irradiance at equinox conditions with a solar constant of $1,365 \text{ W m}^{-2}$ is used. The sea surface temperature (SST) was prescribed zonally uniform and symmetric about the equator and was obtained from the Southern Hemisphere observed climatology. Zonally uniform sea ice fraction was also prescribed where the SST is under the freezing temperature. The model atmosphere was started from arbitrary state of other aqua planet simulation, and initial 180-day period out of 3 year simulations were discarded because of an adjustment period.

In addition to control (EXPctl) simulation, three sensitivity experiments are performed (Table 1). In easterly shear momentum forcing experiment (EXPemf), we vertically perturbed zonal momentum by adding prescribed forcing (Fig. 1a) in every time step. The forcing is imposed in the region of 120E–180E, 5S–5 N. The reason for particularly selecting this region is explained in Sect. 4. Note that our conclusion is quite robust to the size of the forcing domain. In the second one, we did sensitivity experiment (Fig. 1b) with only low level momentum forcing (EXPlmf) to examine the relative effects of wind shear and mean westerly on the simulated HF atmospheric activity. Lastly, we did one more sensitive experiment by prescribing vertically uniform momentum forcing (EXPumf, Fig. 1c) over the same region. The last experiment is aimed to focus on the effect of horizontal shear, by eliminating the vertical shear in momentum forcing.

The response of HF wind variability to the prescribed zonal momentum forcing is examined through the above suite of experiments. In the sensitive simulations, it is found that the model states (wind and mass field) are quickly adjusted to the steady momentum forcing (within 15 days) and they show a balanced state. We also, checked that there is no significant drift of the model state, in spite of steady momentum forcing. Therefore, this facilitates us to regulate the LF wind variability through different momentum forcing scenarios. One advantage of this simplified framework used here is that it can exclude possible effects from zonal SST gradient and land–sea contrast on HF and LF wind variability.

Table 1 Experimental designs using idealized AGCM

Expt	Momentum forcing
EXPemf	Vertically perturbed zonal momentum forcing over the region (120E–180E, 5S–5N) shown in Fig. 5b. The vertical profile of the forcing is as shown in Fig. 1a
EXPlmf	Momentum forcing (as shown in Fig. 1b) over the same region, but only at low level
EXPumf	Momentum forcing (see Fig. 1c) over the same region but with uniform forcing in all levels

**Fig. 1** Vertical profile of the momentum forcing for (a) EXPemf and (b) EXPlmf and (c) EXPumf simulations. EXPemf, EXPlmf and EXPumf are as defined in the text

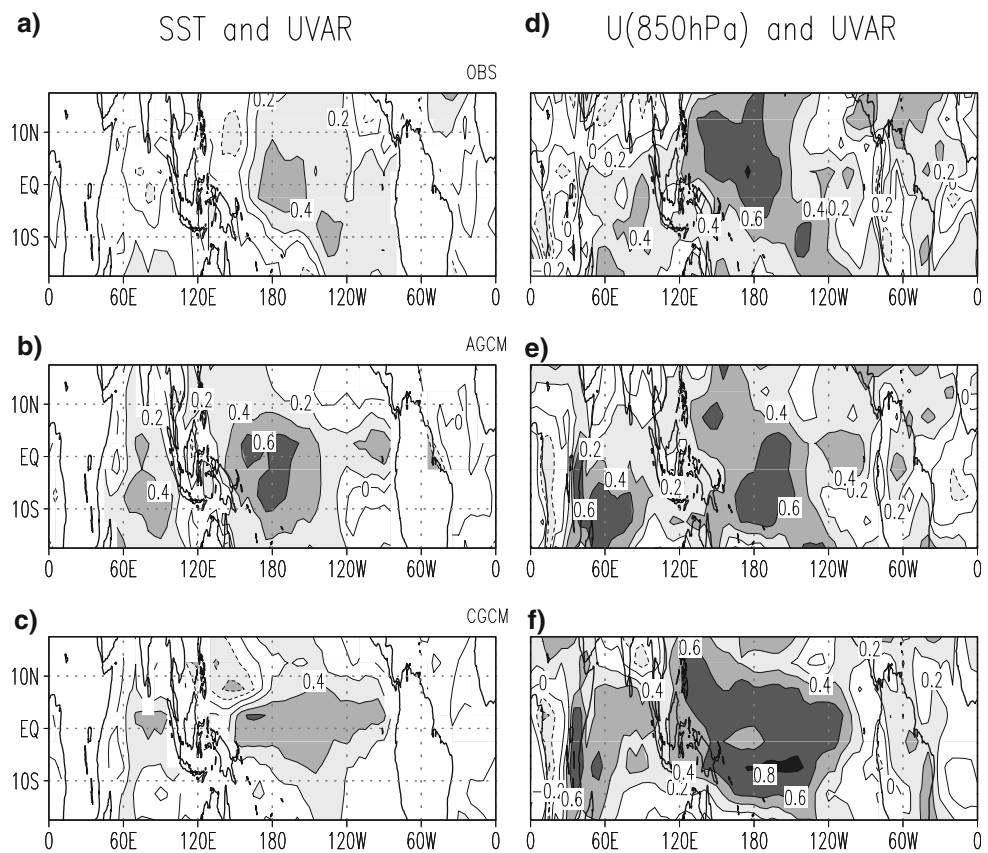
3 Relationship of HF atmospheric variability with large scale circulation

Kug et al. (2008a), recently, showed that the interannual variability of the HF atmospheric variance is highly dependent on the phase of ENSO by showing a lead–lag correlation between NINO3.4 SST (anomalous SST averaged over 170–120°W, 5°S–5°N) and the equatorial HF variance. They found a distinct relationship between ENSO and HF atmospheric variability over the western and central Pacific. Kug et al. (2008b) further examined the model simulations of HF atmospheric variability and its dependency on the El Niño phase. They showed that low-level wind is a crucial component in HF atmospheric variability. So they suggested that HF atmospheric variability is more related to LF zonal wind than to SST. Their results show that, the El Niño related background westerlies allows favorable conditions for strong activity of the atmospheric transient zonal wind anomalies in the equatorial Pacific.

The above lead–lag relation show only remote relations associated with ENSO, since they used ENSO indices. However, it will be interesting to examine how the local SST and circulation affects the HF atmospheric variability. In order to understand the large scale relationship more clearly, we analyzed the local correlation pattern (calculated for every grid point locally) of HF atmospheric variance with 850 hPa zonal wind anomaly and SST anomaly, after interpolating each of them to a coarse resolution of 5 lon. × 5 lat. degrees.

We begin our analysis by looking at the local correlation patterns of SSTA with respect to HF variability using observation. Figure 2a shows the spatial pattern of local correlation. This shows overall positive correlation over the tropical oceans except north equatorial Indian Ocean and the western Pacific. This indicates that the warmer SST is related to stronger activity of the HF atmospheric variability, consistent with previous studies. However, the positive correlation is overall weak and stronger relation is

Fig. 2 *Left* correlation of HF atmospheric variance with respect to SST anomalies from (a) observation, (b) AGCM and (c) CGCM simulations. *Right* correlation of HF atmospheric variance except for that with respect to 850 hPa zonal wind anomaly from (d) observation, (e) AGCM and (f) CGCM simulations. The correlation coefficients of more than 0.2 are shaded



only found over the central Pacific where ENSO variability dominates.

We then calculated the local correlation using 850 hPa zonal wind anomaly, instead of SST (Fig. 2d). Interestingly, correlation coefficients over the whole tropical domain are enhanced now. In particular, a distinctive relationship between HF atmospheric variability and 850 hPa zonal winds is found over western and central Pacific. The correlation coefficients over these regions have increased significantly to over 0.6, with 99% of confidence level. It should be noted that the significant correlation is found not only over the tropical Pacific but also over Indian Ocean and Atlantic Ocean. For example, over southern Indian Ocean and north Atlantic, it shows some relationship, with correlation values of 0.4. Hence, on the basis of observation it is seen that HF atmospheric variability is more strongly related to large scale zonal wind patterns than to SST anomalies.

We then tried to see how the present climate model simulates the above relation. To check this, the same analysis is applied to the simulation of AGCM and CGCM. Figure 2b and e shows these correlation patterns for AGCM. Compared to observation, it shows stronger relationship between SSTA and HF atmospheric variability (Fig. 2b), especially over central pacific region and southern Indian Ocean region. However, when correlated

with zonal wind, it is still consistent with the observation that the overall correlation pattern is enhanced and broadened.

Figure 2c and f shows the correlation for the CGCM. Compared to the AGCM, the CGCM exhibits weaker correlation of SSTA with respect to HF atmospheric variability (Fig. 2c). The correlation over the Pacific is slightly broadened in the simulation as compared to observation (Fig. 2a). Similar to the observation (Fig. 2d), the CGCM simulate relatively strong relation of the HF atmospheric variability with large scale zonal wind (Fig. 2f). In particular, the correlation over Pacific region has increased from 0.5 to 0.7, with 99% significance level. Also over the IO region, the correlation coefficient has increased, even though it shows a broader correlation pattern than observation. This is particularly seen over western and central Pacific region and also in southern Indian Ocean region. However, over north Atlantic basin, it does not simulate the observed relationship. In summary, both the AGCM and CGCM simulate the relatively stronger relation of the HF atmospheric variability with large scale zonal wind, consistent with the observational relation.

Though, we showed a strong relationship between LF and HF atmospheric variability, one may doubt about the above relationship because the zonal wind is also significantly related to the SST. To clarify this problem, we

removed the partial influence of SST and zonal wind on the HF atmospheric variance, respectively. To do this, we introduce the partial correlation (Cohen and Cohen 1983) technique. Recently, this method is frequently used in climate studies, in particular, on the Indian Ocean and ENSO variability (e.g. Kug and Kang 2006). The partial correlation is calculated by excluding the effects of the SST anomaly and 850 hPa zonal wind anomaly, respectively. Figure 3 shows the partial correlation in the observation and in two model simulations. When the effect of the zonal wind is linearly removed, the partial correlation between SST anomaly and HF atmospheric variance shows, interestingly, a weaker correlation both in the observation (Fig. 3a) as well as in all two simulations (Fig. 3b, c). The observed correlation over the east of central Pacific, as seen in Fig. 2a, is disappeared by excluding the effect of zonal wind. Also in the AGCM simulations (see Fig. 3b), the correlation has decreased significantly, in particular, over central Pacific region and also in Indian Ocean region. In the CGCM (Fig. 3c) the removal of effect of zonal wind is quite agreement with the observed pattern of almost null correlation. This is remarkably shown over the whole Pacific region with no significant correlation.

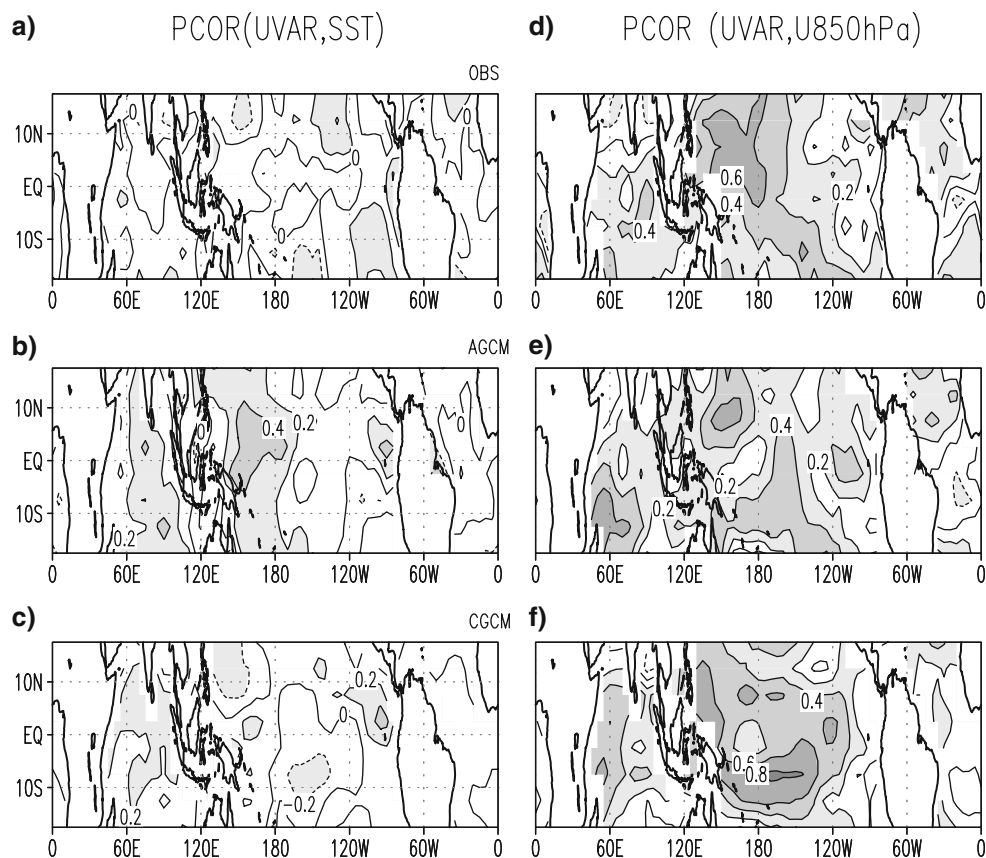
When the effect of SST anomaly is removed in the observation, on the other hand, the zonal wind shows a remarkable stronger relation with the HF atmospheric

variability, especially over the western and central Pacific region (see Fig. 3d). By removing the effect of SST anomaly, the significant correlation is found over Indian and Atlantic Ocean as well, though it is reduced slightly compared to Fig. 2d. AGCM also shows stronger relation (Fig. 3e), though the correlation coefficient is reduced compared to Fig. 2e. However, it still shows higher correlation over north-western Pacific. Similar to observation, CGCM exhibits some stronger relation (Fig. 3f), but there is an eastward and southward extension in the correlation patterns. Also here, the correlation coefficient is slightly reduced compared to Fig. 2f. In summary, this again indicates that the HF atmospheric variability is directly related to LF zonal wind, both in observation as well as in climates models.

4 Idealized modeling experiments

It is seen from earlier section that statistically HF atmospheric variability is more related to LF wind anomaly than to large scale SST anomaly. This relation holds more robust, especially, in western to central Pacific region. However, statistical analyses have always some limitations. For example, a statistical analysis such as partial correlation, cannot completely separate out the effect of

Fig. 3 *Left* partial correlation of HF atmospheric variance with respect to SST anomalies, by removing the effect of zonal wind from (a) observation, (b) AGCM and (c) CGCM simulations. *Right* partial correlation of HF atmospheric variance except for that with respect to 850 hPa zonal wind anomalies, by removing the effect of SST from (d) observation, (e) AGCM and (f) CGCM simulations. The correlation coefficients of more than 0.2 are shaded



wind and SST from each other. It is just a linear assumption to remove the effect of one variable on the other. So far, we do not have any other statistical tools and methods to effectively remove such affects, linearly. So it is difficult to ascertain the role of LF wind anomaly on HF atmospheric variability, solely based on statistical analysis.

However, idealized model experiments with some simplified frameworks can serve this purpose to some extent. In our idealized aqua-planet experiments, the effect of zonal SST gradient is removed by prescribing zonally uniform SST. We prescribed the westerly momentum forcing over 120–180E, 5S–5 N, where the relation of HF atmospheric variability with LF wind is found to hold robust (Fig. 3d). In this section, we will show analyses based on the idealized aqua experiments (see Sect. 2a for a detailed description of these experiments). The results shown here support our statistical relationships, (shown in the above section), makes it more robust.

Figure 4a and b shows the time mean vertical structure of simulated zonal wind field along the equator in the EXPctl and EXPemf, respectively. The zonal wind distribution in the EXPctl experiment shows lower level easterlies and upper level westerlies (Fig. 4a). The prescribed momentum forcing fully modifies the whole vertical structure in the EXPemf (Fig. 4b). In particular, there is a drastic change in the vertical structure, over the forced domain (thick line box in Fig. 5b) with westerly dominating in the lower level. We show further the differences of the EXPemf from EXPctl, in Fig. 4c. This clearly reveals dominant westerlies in the lower levels (confined mainly below 500 mb level) and enhanced easterlies in the upper levels, indicating easterly vertical shear. This also shows an upper level (above 500 mb level) increase in westerly over the far western side of the forcing.

Figure 5 shows the horizontal distribution (at 850 hPa level) of time mean of “LF zonal wind” (defined as 90 day running mean) and “HF zonal wind” (defined as deviation from this 90 day running mean) variance. Hereafter, “HF” refers to this deviation in this study. Strongest LF westerlies manifest in the EXPemf over the forced region. Note that, stronger HF variance (Fig. 5e) coincides with these LF westerlies. The response of the large scale forcing to generate eddies are readily identified from the difference (EXPemf – EXPctl) in LF zonal wind and HF zonal wind variance (Fig. 5c, f).

It will be interesting to see the detailed spectrum (space–time) of this HF variability, since its spatial and temporal scales are important in effectively modulating a coupled system. This analysis will also help us to see whether the spatial and temporal scale of HF variability has changed significantly with momentum forcing. For effectively evaluating and characterizing the HF atmospheric

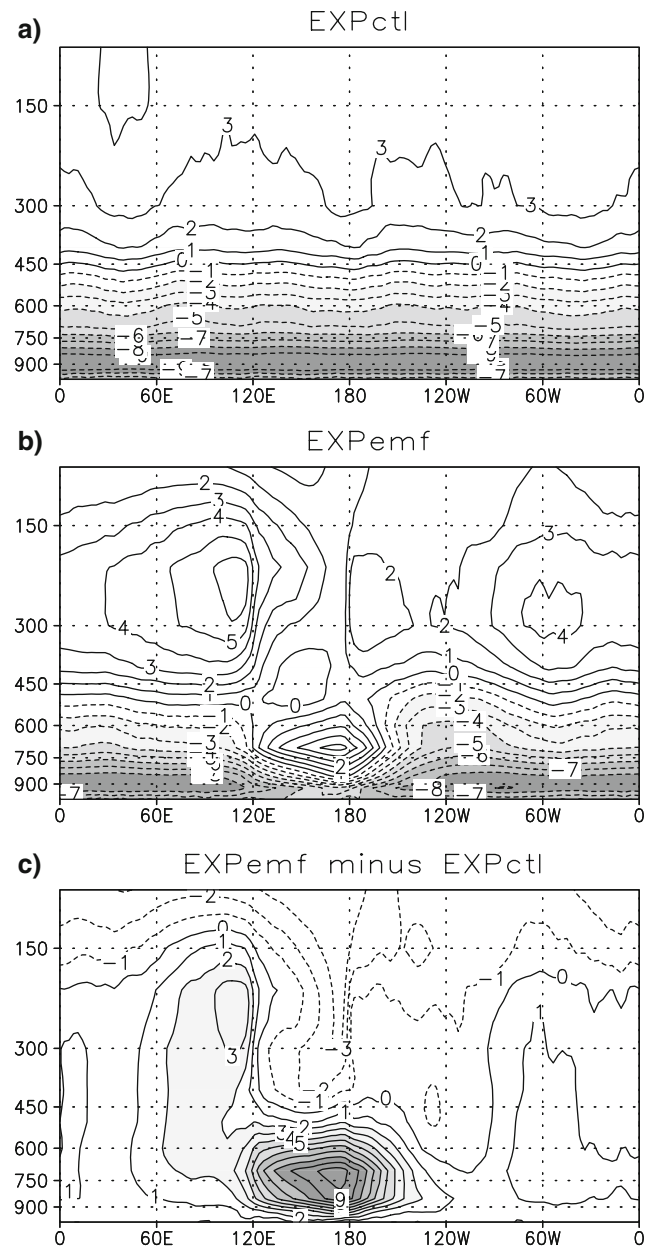
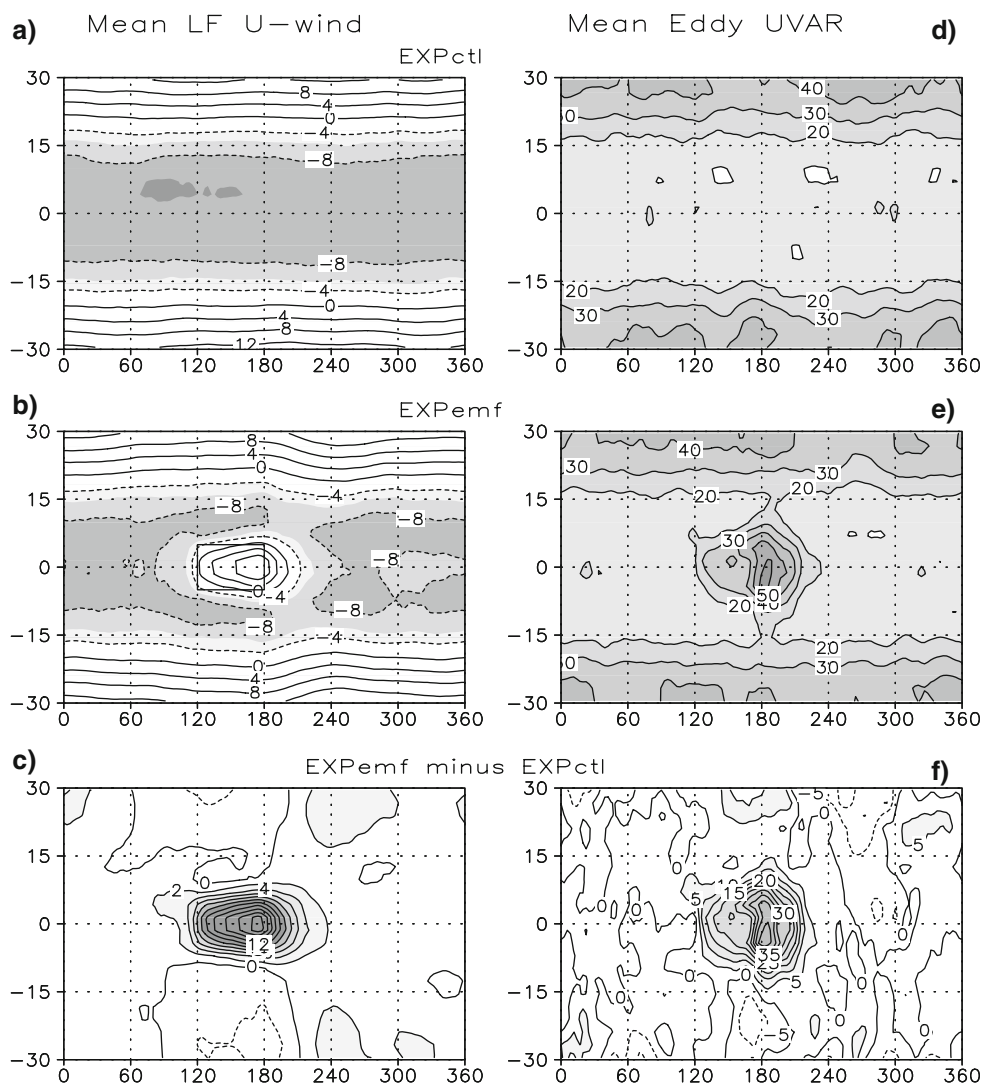


Fig. 4 Time mean vertical structure of zonal wind field along the equator for (a) EXPctl, (b) EXPemf and (c) Difference of EXPemf from EXPctl

variability, we applied wavenumber–frequency spectral analyses (Hayashi 1982) to zonal wind at 850 hPa level, after averaging over all longitudes and along Equator (10S–10N). See the figure caption for more details. The difference between EXPemf and EXPctl in power spectra are shown in Fig. 6. In general, with the momentum forcing, it shows enhanced spectral powers in the 20–90 day period (eastward propagating component). In particular, it shows enhanced spectral powers (of $0.01 \text{ m}^2 \text{ s}^{-2}$) at the wave numbers 1–4 (centered around 30–50 days). Maximum amplitude (of $0.01\text{--}0.02 \text{ m}^2 \text{ s}^{-2}$) is also seen at wave

Fig. 5 Time mean distribution of LF zonal wind at 850 hPa (LF is defined as 90 day running mean) for (a) EXPctl, (b) EXPemf and (c) difference of EXPemf from EXPctl. In (d), (e), (f) same, but for 850 hPa HF zonal wind (defined as deviation from the 90 day running mean) variance



numbers 5–7 (centered around 20–25 days). This leads us to speculate that the stronger HF (<90 days) atmospheric variability in EXPemf as compared to EXPctl, has come mainly from intraseasonal (including MJO) time scale.

How LF wind changes the HF variance patterns so dramatically? For answering this, we calculated the mean (in time) vertical shear (as defined in the figure captions), zonal convergence and meridional shear of LF zonal wind in both simulations (EXPctl and EXPemf). The differences (EXPemf – EXPctl) of these are shown in Fig. 7a, b, and c. HF variance (shaded regions) is also displayed here for comparison. First, it is to be noted here that the stronger variance coincides with easterly vertical shear of the LF zonal wind (Fig. 7a). However, the detail structure of the HF variance is shifted to the east from the vertical shear maximum. It is seen that strong generation of HF variance occurs where the longitudinal zonal wind gradient is strong (Fig. 7b). It is also seen to coincide with latitudinal gradients (Fig. 7c). Therefore, the generation of strong

variance is related to both zonal and meridional shear of the basic state and the maximum generation of HF variance coincides with cyclonic shear of the basic-state LF zonal wind. Earlier, Maloney and Hartmann (2001) showed using EKE budget analysis that both zonal and meridional convergence are equally contributing to the western Pacific tropical cyclone genesis. Further, this is consistent with barotropic wave accumulation by the mean flow, which was noted in previous studies (e.g. Holand 1995; Sobel and Bretherton 1999).

Our results are quite similar to the argument by Seiki and Takayabu (2007b). According to them the LF environmental westerlies centered near the equator provide strong zonal convergence and meridional shear, resulting in favorable conditions for synoptic eddy development. So small scale slow moving eddies are found to grow through barotropic conversion from the mean flow.

To see this more clearly, we calculated HF variance as a function of zonal wind vertical shear (see figure captions)

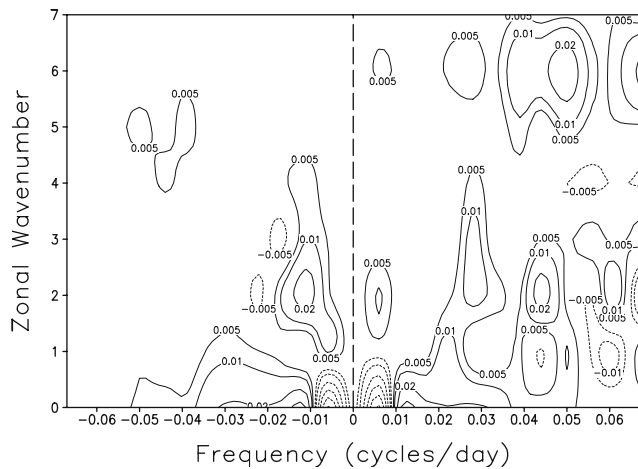


Fig. 6 Difference (between EXPemf and EXPctl) in wavenumber–frequency spectra of 850 hPa zonal wind. Individual spectra were calculated for each 180 day segment (neighborhood segments share 160 days overlaps), and then averaged over all period of data. Only the time mean (for the full period) is removed before calculating the spectra. Units for the spectrum are $m^2 s^{-2}$ per frequency interval per wave number interval. The bandwidth is 180 per day. Zero lines are not drawn

over the equatorial Pacific Ocean (5S–5N, 120E–90W). The daily data sets were organized by zonal wind shear values in to bins of size $0.5 m s^{-1}$. We applied this procedure to both EXPctl and EXPemf simulation for a 90 day moving window. An average HF variance and zonal wind vertical shear is calculated for each bin and is shown in Fig. 8a for EXPemf. HF variance over the Pacific is considerably higher during the easterly vertical shear phase than the westerly shear. So, the dependence of HF variance on the low level wind westerly forcing is clearly manifested in EXPemf. Similarly, we obtained HF variance as a function of zonal wind (at 850 hPa) convergence over the equatorial Pacific Ocean (5S–5N, 120E–90SW). An

average HF variance and zonal wind convergence is calculated for each bin and is shown in Fig. 8b. It clearly shows that stronger variance coincides with low level convergence of westerlies. We found that this tendency is observed even in EXPctl simulation though the range of the wind variation is relatively narrow. We applied the same analysis to observation (HF variance is defined at 850 hPa level) and it is shown in Fig. 8c and d. It shows similarity to our sensitivity experiment (EXPemf), with the dependence of stronger variance on the easterly vertical shear (Fig. 8c) and low level convergence (Fig. 8d), even though, our experiment simulates a larger variance compared to observational one. In the observation, we obtained similar results by defining HF variance at 925 hPa level, but we retained 850 hPa level here mainly to get equivalence with the relatively stronger variance found in the model; our basic results in characterizing the eddy-large scale interaction will not have substantial changes with this HF variance definition.

To show further the impact of the vertical shear more clearly, we conducted additional sensitivity experiment (the EXPImf and see Sect. 2c for details of the experiment) by imposing only lower part of momentum (see Fig. 1b) forcing over the same region (as marked in Fig. 6b) to examine the relative effects of vertical wind shear and mean westerly on the simulated atmospheric HF activity. For the EXPemf and EXPImf, we then calculated the differences from the EXPctl in HF zonal wind variance along the equator and displayed in Fig. 9a. For comparison, we also showed the differences in zonal wind response and its vertical shear in Fig. 9b and c. It is clear from the figure that the difference in the simulated variance is higher in the EXPemf as compared to the EXPImf (Fig. 9a). Also, it shows that over the western part of the forcing, the difference in simulated HF activity is more robust in EXPemf

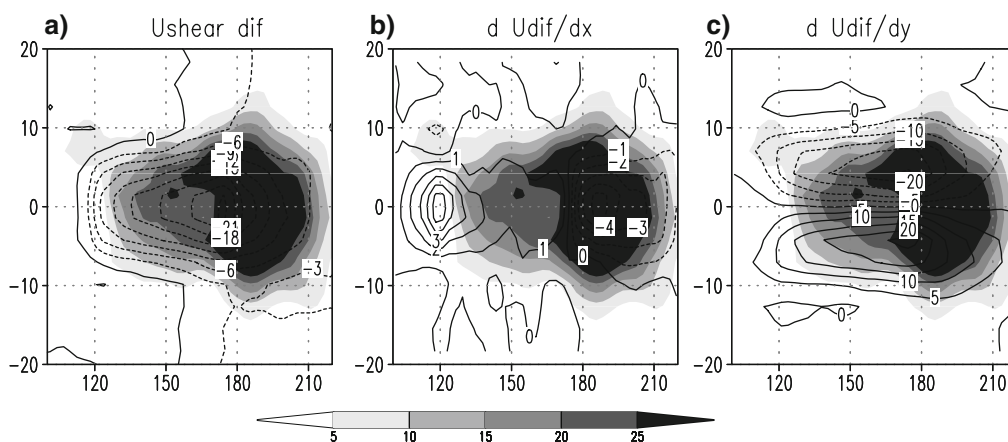
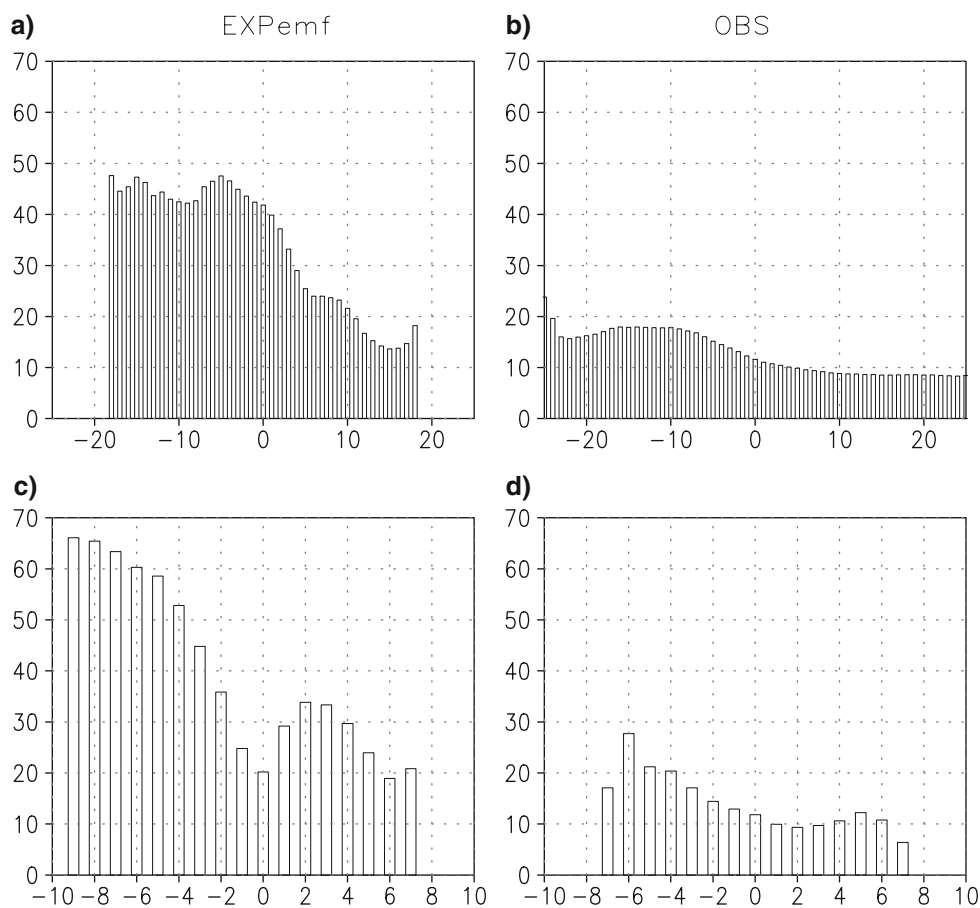


Fig. 7 Time averaged (difference between EXPemf and EXPctl) (a) vertical, (b) zonal and (c) meridional shear of LF zonal wind. For comparison, HF variance (*shaded region*) is also displayed in all

figures. Vertical shear is defined as difference in zonal wind between 200 and 850 hPa level

Fig. 8 HF variance as a function of zonal wind vertical shear over the equatorial Pacific Ocean (5S–5N, 120–270E) for (a) EXPemf and (c) observation. In (b) and (d) same, but as a function of zonal wind convergence at 850 hPa level. See the caption of Fig. 7 for the definition of vertical shear. Units along x -axis and y -axis are in m s^{-1} and $\text{m}^2 \text{s}^{-2}$, respectively



as compared to the EXPlmf. This is noticed especially along 145E, with 35% increase of variance in EXPemf from the EXPlmf. This shows that based on our experiment, the increase of HF variance is due to the effect of vertical shear. Again, in EXPemf simulation, especially near 180E, there is 30% increase in the variance as compared to the EXPlmf. It is to be noted here that variance in EXPlmf is less compared to EXPemf, even though the EXPlmf simulates larger low level westerlies (Fig. 9b). However, the simulations of larger easterly vertical shear in EXPemf (Fig. 9c) as compared to the EXPlmf, underlie the importance of the vertical shear in causing the HF activity.

In order to reveal the role of vertical shear more clearly, we designed another experiment (the EXPumf and see the Sect. 2c) to focus only on the effect of horizontal shear, thus eliminating vertical shear. This is shown in Fig. 9a, b and c marked with dotted lines. The difference in the simulated variance from the EXPctl shows that the simulated variance is lower in the EXPumf as compared to both EXPemf and EXPlmf. It further shows that over the western part of the forcing, the difference in the simulated HF variance is considerably reduced as compared to the EXPemf. This is seen particularly near 145E, where the variance in the EXPumf is

decreased by 60%, as compared to EXPemf. Also, in the western part of the forcing, the EXPumf simulates relatively larger low level westerlies (Fig. 9b), in contrast to its relatively lower variance. This indicates that the absence of the vertical shear in EXPumf simulation is responsible for its lower variance.

These results clearly manifest that vertical shear is also an important parameter in enhancing the HF variance. Regarding this, earlier, Wang and Xie (1996) showed theoretically that transient atmospheric moist Rossby waves are strongly excited in the low level, under background easterly vertical shear. Our results somewhat coincides with this. But at present, we are not sure whether horizontal shear or vertical shear is more important in causing this HF activity. Our results indicate that both components have a crucial role in intensifying HF atmospheric variability. In terms of relative contribution, further studies are needed.

5 Summary and discussion

Relationship of HF atmospheric variability with large scale circulation is studied here. We found that atmospheric HF

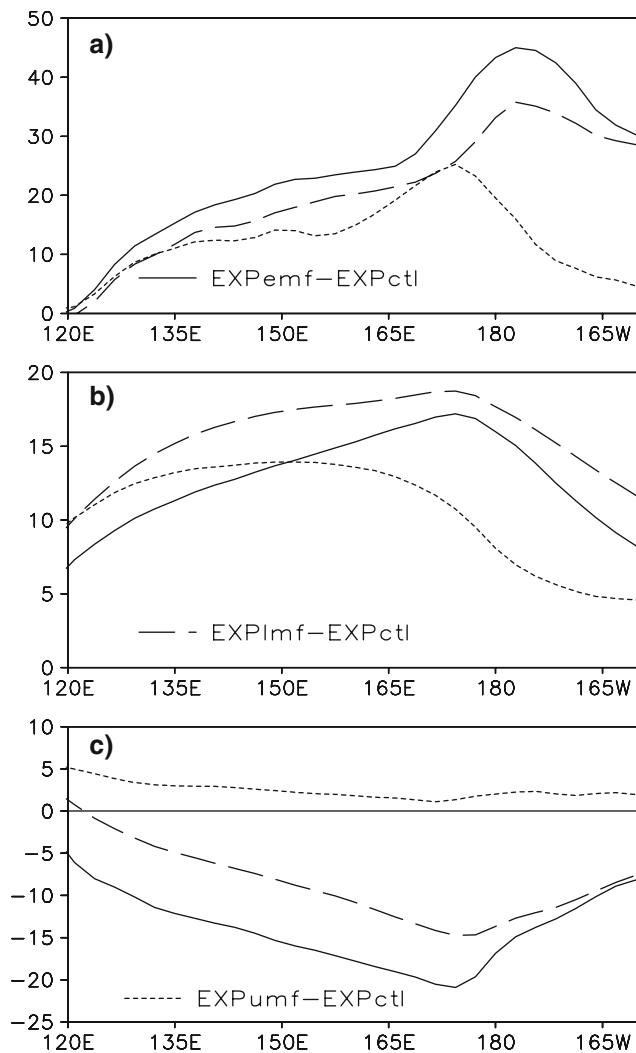


Fig. 9 The difference of equatorially averaged (a) HF zonal wind variance, (b) 850 hPa zonal wind (c) vertical shear of zonal wind for EXPpemf (solid line), EXPlmf (dashed line), EXPpumf (dotted line) from EXPctl. See the caption of Fig. 7 for the definition of vertical shear. Y-axis is in $\text{m}^2 \text{s}^{-2}$ units

variability is more strongly tied to large scale zonal wind patterns than to SST anomalies, using observation and climate models (both atmospheric and coupled models). A distinctive relationship between atmospheric high and low frequency variability is found over tropical Pacific, especially over the western and central Pacific. However, these results are subjected to the limitation of statistical analysis. In order to understand it better, we conducted aqua planet AGCM experiments by prescribing zonal momentum forcing over the selected equatorial region. The response of the large scale forcing to generate HF activity is clearly demonstrated in our experiments.

This study shows that the stronger variance coincides with easterly vertical shear of the LF zonal wind (Fig. 7a). It also manifests the relative importance of horizontal zonal

wind shear, in enhancing the HF variance. This is clearly seen in the eastern part of the westerly momentum forcing, where the HF activity shows relatively maximum value, in spite of similar vertical shear over the forced regions (see Fig. 7). The HF energetic atmospheric variability is found to grow through strong low-level convergence and horizontal shear. As pointed out earlier by Maloney and Hartmann (2001), our experiment (EXPpemf) also reveals that both zonal and meridional shear is related to the generation of strong HF activity over the western to central Pacific regions.

The phase of westerly vertical shear is found to be characterized by less variance (Fig. 8a). The detailed impact of the vertical shear on enhancing the HF activity is also revealed here, through additional sensitive experiments (EXPlmf and EXPpumf). This is clearly seen (see Fig. 9a, c) in the western part of the forcing where HF activity is found to increase in EXPpemf, as compared to both EXPlmf and EXPpumf. The increase in HF variance (in spite of the reduced horizontal shear here, see Fig. 7) over this region is due to the effects of vertical zonal wind shear (see Fig. 9a, c) as described in Sect. 4.

Our results clearly manifest that the vertical and horizontal shear in the zonal wind are important parameters in enhancing the HF variance. Our results partly coincide with Wang and Xie (1997) and Xie and Wang (1996). According to Xie and Wang (1996), a fundamental impact of the vertical shear on the equatorial Rossby wave is that a westerly (easterly) vertical shear favors trapping wave kinetic energy to the upper (lower) troposphere. The enhancement of HF activity in our experiments may be partly due to this. However, at this stage, it is difficult to quantitatively investigate the relative contribution of both horizontal and vertical shears. Therefore, further studies are needed again in this direction.

Apart from the above, to some extent, the present study has an implication on El Nino onset problem. It is still unclear how El Nino events are triggered during boreal spring time. Earlier studies have showed the importance of short-term atmospheric variability (Luther et al. 1983; McPhaden 1999; Perigaud and Cassou 2000; Curtis et al. 2004; Lengaigne et al. 2004) and anomalous western Pacific westerlies (Weisberg and Wang 1997; Kug et al. 2005) to the onset of El Nino. In this regard, our study showed that the two components, HF atmospheric variability and anomalous westerly wind are closely correlated to each other, indicating that we can consider both components as a same factor. Thus, the anomalous westerlies with stronger HF atmospheric activity can be good a precursor for the onset of El Nino.

So far, MJO simulation seems to be a difficult endeavor for global climate models. A scrutiny of GCMs a decade ago revealed that their abilities of simulating the MJO were

very limited (Slingo et al. 1996; Sperber et al. 1997). The most common problems in MJO simulation are weak eastward propagating signals, too large phase speed and unrealistic seasonal cycles. In this regard, recently, Zhang et al. (2006), has compared simulations of the MJO in four pairs of coupled and uncoupled global climate models. Their diagnostics supports the notion that MJO simulation might be related to its background state in terms of mean low-level zonal wind (e.g., Inness et al. 2001) and precipitation (Slingo et al. 1996). Hence, we need better representation of basic climatological flow in model simulations. Our results further support this notion because we showed that the MJO activity depend on the LF circulation. It seems that the current models, to some extent, capture the overall relation between LF zonal wind and MJO variability, as shown in Figs. 2 and 3. This implies that better simulation of climatology and LF variability may help us to improve the MJO simulation skill.

Acknowledgments The work was supported by the SRC program of Korea Science and Engineering Foundation, and Brain Korea 21 Project. F.-F. Jin and J.-S. Kug were partly supported by NSF grants ATM-0652145 and ATM-0650552 and NOAA grants GC01-229. S.-W. Yeh is supported by KORDI (PG47100, PE98004).

References

- Bonan GB (1996) A land surface model (LSM version 1.0) for ecological, hydrological, and atmospheric studies: technical description and user's guide. NCAR tech. note NCAR/TN-417+STR, Natl. Cent. for Atmos. Res., Boulder, Colorado, 150 pp
- Cohen J, Cohen P (1983) Applied multi regression/correlation analysis for the behavioral sciences. Lawrence Erlbaum Associates, Hillsdale, 545 pp
- Curtis S, Adler RF, Huffman GJ, Gu G (2004) Westerly wind events and precipitation in the eastern Indian Ocean as predictors for El Niño: climatology and case study for the 2002–2003 El Niño. *J Geophys Res* 109:D20104. doi:10.1029/2004JD004663
- Duchon C (1979) Lancos filtering in one and two dimensions. *J Appl Meteorol* 1016–1022. doi:10.1175/1520-0450(1979)018<1016:LFI0AT>2.0.CO;2
- Eisenman I, Yu L, Tziperman E (2005) Westerly wind bursts: ENSO's tail rather than the dog? *J Clim* 18:5224–5238. doi:10.1175/JCLI3588.1
- Gebbie G, Eisenman I, Wittenberg A, Tziperman E (2007) Modulation of westerly wind bursts by sea surface temperature: a semi-stochastic feedback for ENSO. *J Atmos Sci* (in press)
- Gutzler DS (1991) Interannual fluctuations of intraseasonal variance of near-equatorial winds. *J Geophys Res* 96:3173–3185
- Hayashi Y (1982) Space–time spectral analysis and its application to atmospheric waves. *J Meteorol Soc Jpn* 60:156–171
- Holand GJ (1995) Scale interaction in the western Pacific monsoon. *Meteorol Atmos Phys* 56:57–79. doi:10.1007/BF01022521
- Holtlag AAM, Boville BA (1993) Local versus nonlocal boundary layer diffusion in a global climate model. *J Clim* 6:1825–1642. doi:10.1175/1520-0442(1993)006<1825:LVNBLD>2.0.CO;2
- Inness PM, Slingo JM, Woolnough SJ, Neale RB, Pope VD (2001) Organization of tropical convection in a GCM with varying vertical resolution: implications for the simulation of the Madden–Julian oscillation. *Clim Dyn* 17:777–793. doi:10.1007/s003820000148
- Jin F-F, Lin L, Timmermann A, Zhao J (2007) Ensemble-mean dynamics of the ENSO recharge oscillator under state-dependent stochastic forcing. *Geophys Res Lett* 34:L03807. doi:10.1029/2006GL027372
- Kalnay E et al. (1996) The NCEP/NCAR 40-year reanalysis project. *Bull Am Meteorol Soc* 77:437–471. doi:10.1175/1520-0477(1996)077<0437:TNYRP>2.0.CO;2
- Keen RA (1982) The role of cross-equatorial cyclone pairs in the Southern Oscillation. *Mon Weather Rev* 110:1405–1416. doi:10.1175/1520-0493(1982)110<1405:TROCET>2.0.CO;2
- Kerr RA (1999) Big El Niños ride the back of slower climate change. *Science* 283:1108–1109. doi:10.1126/science.283.5405.1108
- Kessler WS, Kleeman R (2000) Rectification of the Madden–Julian Oscillation into the ENSO cycle. *J Clim* 13:3560–3575. doi:10.1175/1520-0442(2000)013<3560:ROTMJO>2.0.CO;2
- Kim D, Kug J-S, Kang I-S, Jin F-F, Wittenberg AT (2008) Tropical Pacific impacts of convective momentum transport in the SNU coupled GCM. *Clim Dyn*. doi:10.1007/s00382-007-0348-4
- Kug J-S, An S-I, Jin F-F, Kang I-S (2005) Preconditions for El Niño and La Niña onsets and their relation to the Indian Ocean. *Geophys Res Lett* 32:L05706. doi:10.1029/2004GL021674
- Kug J-S, Kang I-S (2006) Interactive feedback between the Indian Ocean and ENSO. *J Clim* 19:1784–1801. doi:10.1175/JCLI3660.1
- Kug J-S, Jin F-F, Sooraj KP, Kang I-S (2008a) Evidence of the state-dependent atmospheric noise associated with ENSO. *Geophys Res Lett*. doi:10.1029/2007GL032450
- Kug J-S, Sooraj KP, Kim D, Kang I-S, Jin F-F, Takayabu YN et al (2008b) Simulation of state-dependent high frequency atmospheric variability associated with ENSO. *Clim Dyn*. doi:10.1007/s00382-008-0434-2
- Kug J-S, Kang I-S, Choi D-H (2008c) Seasonal climate predictability with tier-one and tier-two prediction systems. *Clim Dyn*. doi:10.1007/s00382-007-0264-7
- Lengaigne M, Guilyardi E, Boulanger JP, Menkes C, Delecluse P, Inness P et al (2004) Triggering of El Niño by westerly wind events in a coupled general circulation model. *Clim Dyn* 23:601–620. doi:10.1007/s00382-004-0457-2
- Le Treut H, Li Z-X (1991) Sensitivity of an atmospheric general circulation model to prescribed SST changes: feedback effects associated with the simulation of cloud optical properties. *Clim Dyn* 5:175–187
- Luther DS, Harrison DE, Knox RA (1983) Zonal winds in the central equatorial Pacific and El Niño. *Science* 222:327–330. doi:10.1126/science.222.4621.327
- Maloney ED, Hartmann DL (2001) The Madden–Julian oscillation, barotropic dynamics and North Pacific tropical cyclone formation. Part I: observation. *J Atmos Sci* 58:2545–2558. doi:10.1175/1520-0469(2001)058<2545:TMJOBOD>2.0.CO;2
- McPhaden MJ (1999) Genesis and evolution of the 1997–1998 El Niño. *Science* 283:950–954. doi:10.1126/science.283.5404.950
- McPhaden MJ (2004) Evolution of the 2002–03 El Niño. *Bull Am Meteorol Soc* 85:677–695. doi:10.1175/BAMS-85-5-677
- Nakajima T, Tsukamoto M, Tsuchima Y, Numaguti A (1995) Modelling of the radiative processes in an AGCM. In: Matsuno T (ed) *Climate system dynamics and modelling*, vol 1–3, University of Tokyo, Tokyo, pp 104–123
- Neale RB, Hoskins BJ (2000) A standard test for AGCMs and their physical parameterizations. I: the proposal. *Atmos Sci Lett* 1:101–107. doi:10.1006/asle.2000.0019
- Noh Y, Kim HJ (1999) Simulations of temperature and turbulence structure of the oceanic boundary layer with the improved near-surface process. *J Geophys Res Oceans* 104:15621–15634. doi:10.1029/1999JC900068

- Numaguti A, Takahashi M, Nakajima T, Sumi A (1995) Development of an atmospheric general circulation model. In: Matsuno T (ed) *Climate system dynamics and modelling*, vol 1–3, University of Tokyo, Tokyo, pp 104–123
- Perez CL, Moore AM, Zavaly-Garay J, Kleeman R (2005) A comparison of the influence of additive and multiplicative stochastic forcing on a coupled model of ENSO. *J Clim* 18:5066–5085. doi:[10.1175/JCLI3596.1](https://doi.org/10.1175/JCLI3596.1)
- Perigaud C, Cassou C (2000) Importance of oceanic decadal trends and westerly wind bursts for forecasting El Niño. *Geophys Res Lett* 27:389–392. doi:[10.1029/1999GL010781](https://doi.org/10.1029/1999GL010781)
- Seiki A, Takayabu YN (2007a) Westerly wind bursts and their relationship with intraseasonal variations and ENSO, Part I: statistics. *Mon Weather Rev* (in press)
- Seiki A, Takayabu YN (2007b) Westerly wind bursts and their relationship with intraseasonal variations and ENSO, Part II: energetics over the Western and Central Pacific. *Mon Weather Rev* (in press)
- Slingo JM, Sperber KS, Boyle JS, Ceren JP, Dix M, Dugas B et al (1996) Intraseasonal oscillations in 15 atmospheric general circulation models: results from an AMIP Diagnostic subproject. *Clim Dyn* 12:325–357. doi:[10.1007/BF00231106](https://doi.org/10.1007/BF00231106)
- Smith TM, Reynolds RW (2004) Improved extended reconstruction of SST (1854–1997). *J Clim* 17:2466–2477. doi:[10.1175/1520-0442\(2004\)017<2466:IEROS>2.0.CO;2](https://doi.org/10.1175/1520-0442(2004)017<2466:IEROS>2.0.CO;2)
- Sobel AH, Bretherton CS (1999) Development of synoptic-scale disturbances over the summertime tropical northwest Pacific. *J Atmos Sci* 56:3106–3127. doi:[10.1175/1520-0469\(1999\)056<3106:DOSSDO>2.0.CO;2](https://doi.org/10.1175/1520-0469(1999)056<3106:DOSSDO>2.0.CO;2)
- Sperber KR, Slingo JM, Inness PM, Lau WK-M (1997) On the maintenance and initiation of the intraseasonal oscillation in the NCEP/NCAR reanalysis and in the GLA and UKMO AMIP simulations. *Clim Dyn* 13:769–795. doi:[10.1007/s003820050197](https://doi.org/10.1007/s003820050197)
- Stevens DE (1979) Vorticity, momentum and divergence budgets of synoptic-scale wave disturbances in the tropical eastern Atlantic. *Mon Weather Rev* 107:535–550. doi:[10.1175/1520-0493\(1979\)107<0535:VMADBO>2.0.CO;2](https://doi.org/10.1175/1520-0493(1979)107<0535:VMADBO>2.0.CO;2)
- Stevens DE, Lindzen RS, Shapiro LJ (1977) A new model of tropical waves incorporating momentum mixing by cumulus convection. *Dyn Atmos Oceans* 1:365–425. doi:[10.1016/0377-0265\(77\)90001-X](https://doi.org/10.1016/0377-0265(77)90001-X)
- Stones PH, Quirk WJ, Somerville RCJ (1974) The effect of small-scale vertical mixing of horizontal momentum in a general circulation model. *Mon Weather Rev* 102:765–771. doi:[10.1175/1520-0493\(1974\)102<0765:TEOSSV>2.0.CO;2](https://doi.org/10.1175/1520-0493(1974)102<0765:TEOSSV>2.0.CO;2)
- Tiedtke M (1983) The sensitivity of the time-mean large-scale flow to cumulus convection in the ECMWF model. Workshop on convection in large-scale numerical models. ECMWF, November 28–December 1 1983, pp 297–316
- Vecchi GA, Harrison DE (2000) Tropical Pacific sea surface temperature anomalies, El Niño and equatorial westerly events. *J Clim* 13:1814–1830. doi:[10.1175/1520-0442\(2000\)013<1814:TPSSTA>2.0.CO;2](https://doi.org/10.1175/1520-0442(2000)013<1814:TPSSTA>2.0.CO;2)
- Wang B, Xie X (1996) Low-frequency equatorial waves in vertically sheared zonal flow. Part I: stable waves. *J Atmos Sci* 53:449–467. doi:[10.1175/1520-0469\(1996\)053<0449:LFEWIV>2.0.CO;2](https://doi.org/10.1175/1520-0469(1996)053<0449:LFEWIV>2.0.CO;2)
- Wang B, Xie X (1997) A model for boreal summer intraseasonal oscillation. *J Atmos Sci* 54:72–86. doi:[10.1175/1520-0469\(1997\)054<0072:AMFTBS>2.0.CO;2](https://doi.org/10.1175/1520-0469(1997)054<0072:AMFTBS>2.0.CO;2)
- Weisberg RH, Wang C (1997) Slow variability in the equatorial west-central Pacific in relation to ENSO. *J Clim* 10:1998–2017. doi:[10.1175/1520-0442\(1997\)010<1998:SVITEW>2.0.CO;2](https://doi.org/10.1175/1520-0442(1997)010<1998:SVITEW>2.0.CO;2)
- Wu XQ, Yanai M (1994) Effects of vertical wind shear on the cumulus transport of momentum—observations and parameterization. *J Atmos Sci* 51:1640–1660. doi:[10.1175/1520-0469\(1994\)051<1640:EOVWSO>2.0.CO;2](https://doi.org/10.1175/1520-0469(1994)051<1640:EOVWSO>2.0.CO;2)
- Xie X, Wang B (1996) Low-frequency equatorial waves in vertically sheared zonal flow. Part II: unstable waves. *J Atmos Sci* 53:3589–3605. doi:[10.1175/1520-0469\(1996\)053<3589:LFEWIV>2.0.CO;2](https://doi.org/10.1175/1520-0469(1996)053<3589:LFEWIV>2.0.CO;2)
- Yu L, Weller RA, Liu TW (2003) Case analysis of a role of ENSO in regulating the generation of westerly wind bursts in the western equatorial Pacific. *J Geophys Res* 108:3128. doi:[10.1029/2002JC001498](https://doi.org/10.1029/2002JC001498)
- Zavala-Garay J, Zhang C, Moore A, Kleeman R (2005) The linear response of ENSO to the Madden–Julian oscillation. *J Clim* 18:2441–2459. doi:[10.1175/JCLI3408.1](https://doi.org/10.1175/JCLI3408.1)
- Zhang C, Dong Min, Gualdi S, Hendon HH, Maloney ED, Marshall A, Sperber KR, Wang W (2006) Simulations of the Madden–Julian oscillation in four pairs of coupled and uncoupled global models. *Clim Dyn*. doi:[10.1007/s00382-006-0148-2](https://doi.org/10.1007/s00382-006-0148-2)